Tropical Pacific Surface Wind Energy Spectra and Coherence: Basinwide Observations and Their Observing System Implications

ANDREW M. CHIODI AND D. E. HARRISON

Joint Institute for the Study of the Ocean and Atmosphere, University of Washington, and NOAA Pacific Marine Environmental Laboratory, Seattle, Washington

(Manuscript received 14 November 2019, in final form 30 March 2020)

ABSTRACT

The tropical Pacific moored-buoy array spacing was based on wind coherence scales observed from low-lying islands in the western-central tropical Pacific. Since the array was deployed across the full basin in the mid-1990s, winds from the array have proven critical to accurately monitoring for decadal-scale changes in tropical Pacific winds and identifying spurious trends in wind analysis products used to monitor for long-term change. The array observations have also greatly advanced our ability to diagnostically model (hindcast) and thereby better understand the observed development of central Pacific sea surface temperature anomaly development associated with El Niño and La Niña events, although the eastern equatorial Pacific is not yet accurately hindcast. The original array-design assumptions that the statistics calculated from the western-central Pacific island records are representative of open-ocean conditions and other regions of the tropical Pacific have not been thoroughly reexamined. We revisit these assumptions using the basinwide wind observations provided by the array and find that key wind statistics change across the tropical Pacific basin in ways that could not be determined from the original island wind study. The island results provided a best-case answer for mooring zonal spacing with minimally redundant coherence between adjacent buoys. Buoy-observed meridional coherence scales are longer than determined from the islands. Enhanced zonal sampling east of 140°W and west of 180° is needed to obtain minimal redundancy (optimal spacing). Reduced meridional sampling could still yield minimal redundancy for wind and wind stress fields over the ocean waveguide.

1. Introduction

Understanding the tropical coupled ocean–atmosphere interactions of El Niño–Southern Oscillation (ENSO) requires knowledge of variability at the air–sea interface, and particularly of sea surface temperature (SST) and surface wind stress. Because of the strong surface currents, moored instruments are well suited for observing the equatorial waveguide where the ENSO interactions are strong. The need for direct observations of winds has been demonstrated by the wide differences in operational wind analyses over the region when direct observations were few (e.g., Harrison et al. 1990; Smith et al. 2001; Wittenberg 2004; Chiodi and Harrison 2017a). A basinwide array of surface moorings was recommended to address this need under the Tropical Ocean Global Atmosphere (TOGA) program and was incrementally deployed (McPhaden et al. 1998, 2010; Ando et al. 2017). The United States and Japan ultimately cosponsored tropical Pacific component of this effort as the TAO/TRITON array.

The TAO/TRITON moored array spacing was based on the observed scales of surface wind observations from low-lying islands in the western-central tropical Pacific (Harrison and Luther 1990). Sampling every 15° of longitude and 2–3° of latitude on subdaily time scales has resolved the unusual and energetic subseasonal variability in zonal wind that is characteristic of westerly wind events (e.g., Keen 1982; Delcroix et al. 1993; Hartten 1996; Harrison and Vecchi 1997; Feng et al. 1998; Vecchi and Harrison 2000; Lengaigne et al. 2004; Eisenman et al. 2005) in that region. The resulting wind fields have demonstrated the utility of the array by providing forcing for successful oceanic hindcasts of Niño-3.4 SSTA (signal-to-noise > 2) over periods when

Supplemental information related to this paper is available at the Journals Online website: https://doi.org/10.1175/JCLI-D-19-0836.s1.

Corresponding author: Andrew M. Chiodi, andy.chiodi@noaa.gov

DOI: 10.1175/JCLI-D-19-0836.1

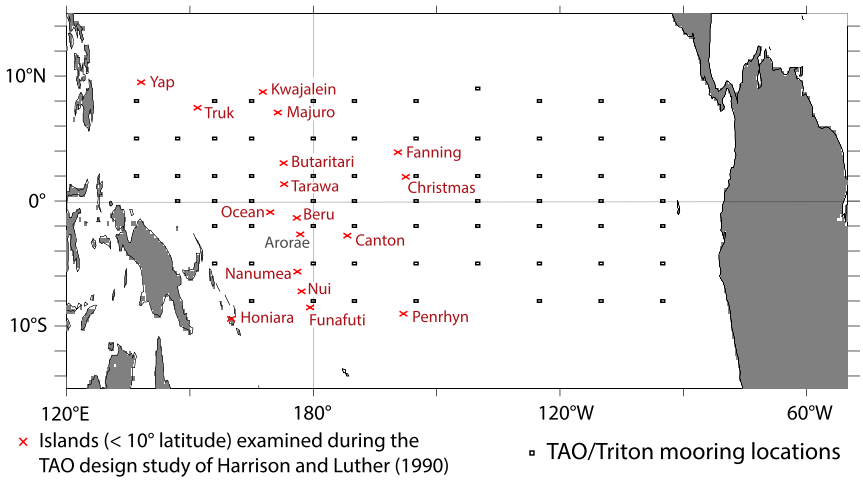

FIG. 1. The traditional TAO/Triton mooring locations (boxes) and equatorial Pacific Islands that provided wind records used in the seminal TAO design studies.

most of the array was returning good wind observations (Chiodi and Harrison 2017b). Winds from the moored-buoy array have also been used to document nontrivial discrepancies in historical ''reanalyses'' of the tropical Pacific winds (Josey et al. 2014; Chiodi et al. 2019).

At present there is interest in reimagining the Tropical Pacific Observing System (TPOS), of which the array is a fundamental element. Figure 1 shows the islands between 10°N and 10°S whose observations provided the basis for previous studies of the variability of surface tropical Pacific winds between ~1950 and 1980. The ''island array'' is limited to the western-central tropical Pacific (Harrison and Luther 1990). Clearly the spatial distribution of the islands limits the area over which spectral density of variance distributions can be evaluated, and the distances over which paired island–wind coherence calculations can be made.

We here make use of continuous data records from the array to reexamine these observed space and time scales of zonal and meridional wind and wind stress variability in the energetic subseasonal (3–60-day period) band. The objectives are to better understand these aspects of the tropical Pacific wind variability field and how the array might be reconfigured for improved monitoring capability and efficiency.

2. Data and methods

We examine two main sets of statistics calculated from the wind observations provided by the Tropical Atmosphere Ocean/Triangle Trans-Ocean Buoy Network (TAO/TRITON 2000) moored-buoy array: the spectral density of variance of the zonal and meridional wind and wind stress components, and the coherence magnitude of these wind components observed at different pairs of moored-buoys. We consider the daily-averaged wind observations reported in near–real time by the TAO/TRITON moored-buoy array over the period 1986–2018. The daily averaged TAO/TRITON winds are based on 10-min averages stored on the buoys. Vandalism and other forms of instrument failure have created gaps in the records provided by each of the buoys that typically last a few months. We use the longest continuous daily averaged record available at each site (or pair of sites in the coherence case) with the criteria that at least 630 and 365 days be available for the spectral density of variance and coherence magnitude calculations, respectively. The coherence minimum (365 days) is shorter than the spectral variance minimum (630 days) because of the added difficulty in finding continuous pairs, as opposed to single-site records. Applying these record-length minimums ensures that at least several 60-day periods are included in each of the results considered.

The Tarawa (1°N, 173°W) zonal wind record featured prominently in the original Harrison and Luther (1990) study. Its enhanced zonal wind energy in the 3–60-day band and peak in the 7–30-day band, documented by Harrison and Luther (1990) based on observations from the 1950s through the 1980s, have been confirmed to be a persistent feature of recent decades by Chiodi and Harrison (2015). Tarawa winds were obtained from Met Office's Hadley Center (HadISD 2009; Dunn et al. 2016) for comparison herein to the nearby moored-buoy results.

Wind stress is estimated from daily averaged observations using the following parameterization for the zonal (τ^x) and meridional (τ^y) components of wind pseudostress:

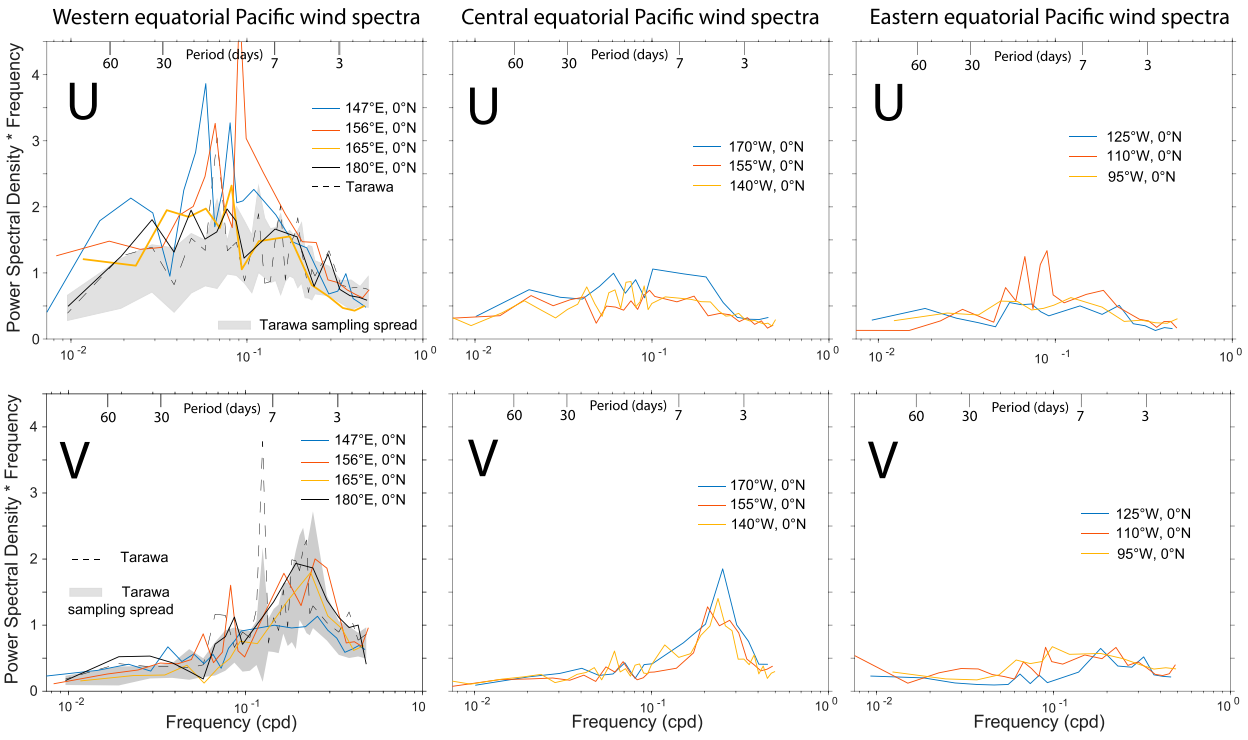

FIG. 2. Spectral density of variance of (top) zonal and (bottom) meridional winds observed by the TAO/TRITON moored buoys along the equator. The longest continuous daily averaged wind records available were used at each moored-buoy site listed. (top left) Tarawa Island wind results are also shown and are based on the Tarawa segment coincident with the longest available 0°, 180° buoy segment (dashed line) and subsampling the Tarawa record by splitting it into unique, same-length segments (shaded curve). The *y*-axis values are in $m^2 s^{-2}$; the *x*-axis values are in cycles per day (cpd).

$$\tau^x = \rho_a C_d |\mathbf{U}| u,$$

$$\tau^y = \rho_a C_d |\mathbf{U}| v,$$

with air density (ρ_a) assigned the value of $1.25\,\mathrm{kg\,m^{-3}}$ and $C_d = 1.3 \times 10^{-3}$; $\mathbf{U}$ is the observed wind vector, $|\mathbf{U}|$ is the observed wind speed, and u and v are the zonal and meridional components of the wind vector, respectively. This formula for estimating wind stress from moored-buoy wind observations was used previously by Harrison et al. (2009) and more recently by Chiodi (2019) to produce realistic ocean model simulations of the upper tropical Pacific seasonal cycle of currents and temperature and the central Pacific SSTA development observed during recent (1992–2017) El Niño and La Niña events.

The spectral density of variance (energy per frequency band) of zonal and meridional wind and wind stress was estimated using the now long-standing approach of calculating the complex conjugate of the discrete Fourier transform of the given wind or wind stress component (Bracewell 1978). Time means were removed and end points matched (tapered to zero anomaly) with a half-period cosine function applied over the first and last 5% of the records prior to calculation of the Fourier transform. The raw spectral densities of variance estimates were smoothed over m adjacent and independent frequency bands to increase statistical stability of the resulting wind spectra, with $m = 8$ for frequencies lower than 0.1 cycles per day (cpd), and $m = 25$ for frequencies higher than 0.1 cpd.

The coherence q between records from pairs of moored buoys, i and j, was calculated based on the spectral (G^m_{ii} and G^m_{jj}) and cross-spectral density of variance G^m_{ij}, averaged over m adjacent frequency bands, as (see Bendat and Piersol 1971)

$$q = \frac{G^m_{ij}(f)}{\sqrt{G^m_{ii}(f) G^m_{jj}(f)}},$$

with m varying from 8 to 25 bands depending on frequency, as in the spectral energy case. Note that q is a complex number whose absolute value provides an estimate of the coherence magnitude between wind records i and j in a given frequency band. The angle between its real and imaginary parts quantifies the phase between records i and j in a given frequency band. The 95% confidence intervals of coherence magnitudes were

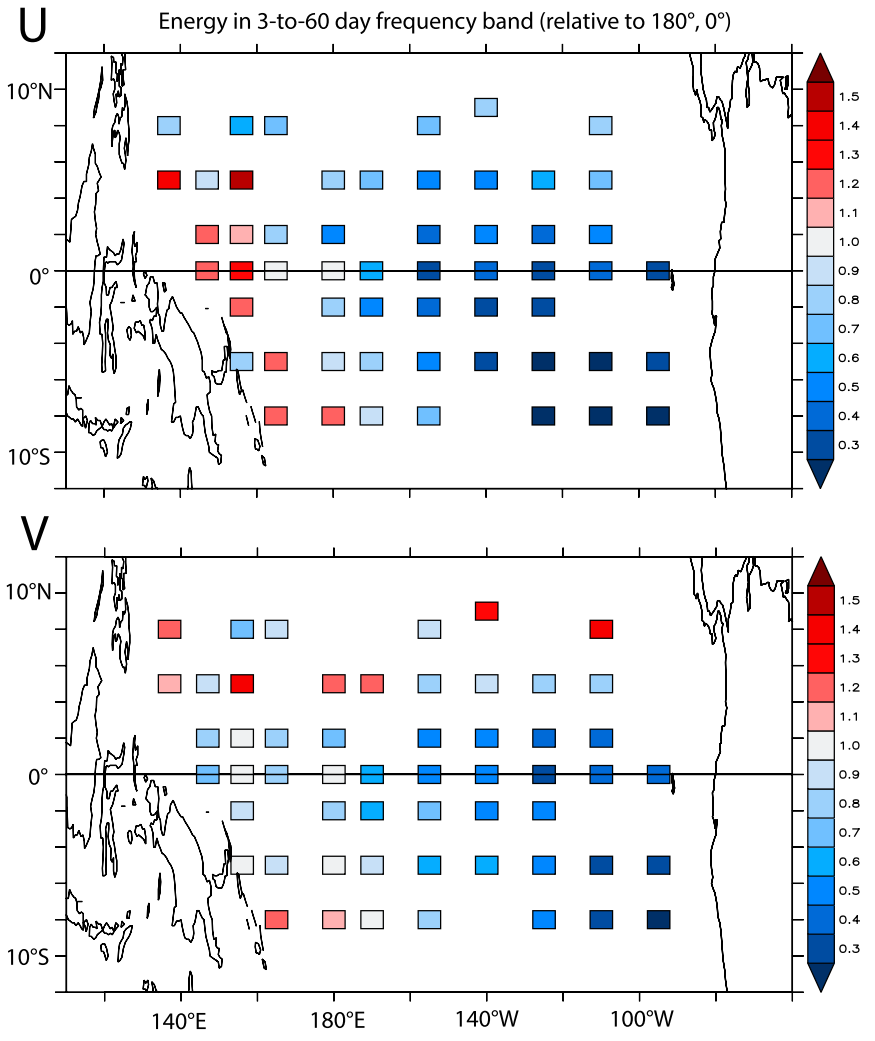

FIG. 3. Mean energy (power spectral density times frequency) in the 3–60-day frequency band relative to the moored-buoy result at 0°, 180°.

calculated using Monte Carlo methods ($n = 10\,000$) in which one of the records was randomly subsampled with replacement and the resulting library of random results used to estimate the likelihood of reaching the $p = 0.05$ coherence magnitude by chance.

3. Results

a. Wind energy spectra

Wind spectral density of variance results from the moored-buoy observations along the equator at 147°E, 156°E, 165°E, and 180° are compared with results from the same periods at Tarawa (1°N, 173°E) in the top-left panel of Fig. 2. Each of these western Pacific to the date line region buoy records show enhanced zonal wind variance within the 7–30-day range. This enhancement is even larger at the westernmost buoys than exhibited in the Tarawa record; 147° and 156°E exhibit approximately 50% more 7–30-day zonal wind variance than 180°, which in turn exhibits ~10% more 7–30-day variance than Tarawa. The 165°E record exhibits ~10% more zonal wind variance than 180°.

The meridional wind records from these mooring sites (Fig. 2; bottom-left panel) all show enhanced variance in the 3–10-day band, as does the Tarawa record. The Tarawa subsegment coincident with the longest continuous 180° record, as well as 10% of those used to calculate the Tarawa spread, exhibits a peak at a period of 8 days, which is not seen in the buoy records. More study is needed to understand the origin and intermittency of this island wind peak.

Due to gaps in the buoy records we are not able to compare the percentage of energy in these <60-day

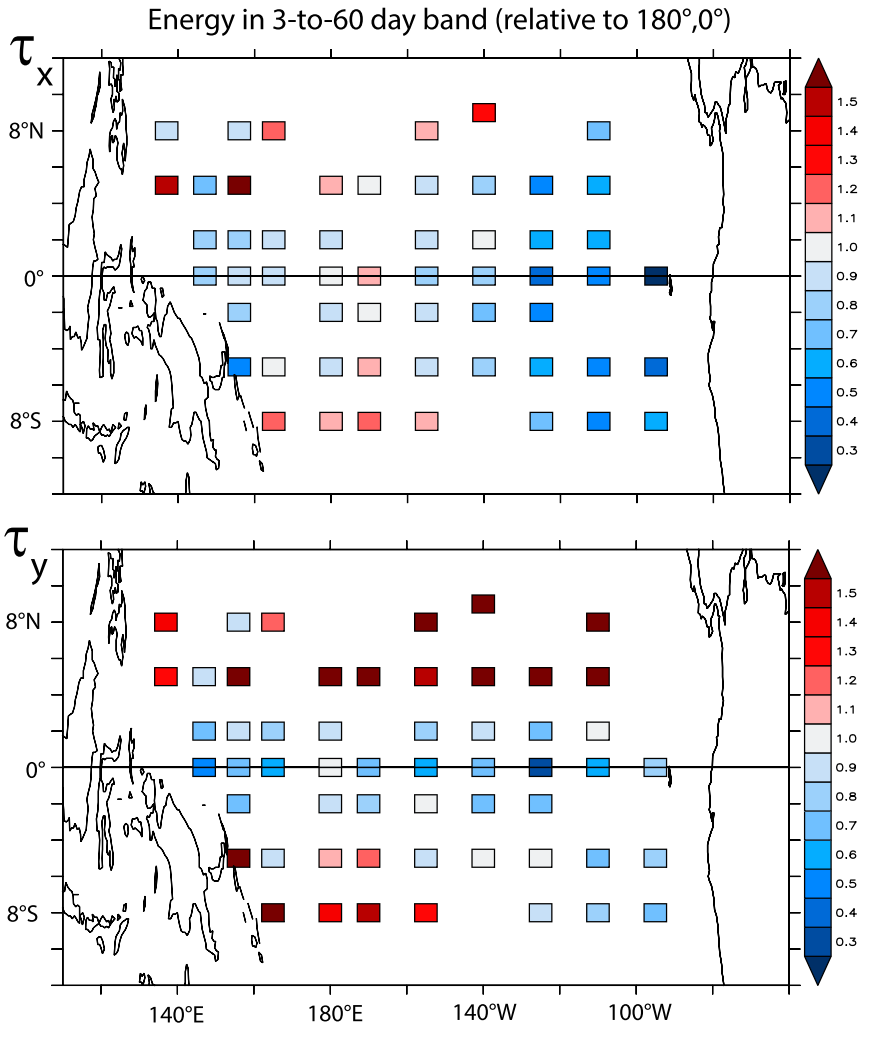

FIG. 4. As in Fig. 3, but for (top) zonal and (bottom) meridional wind stress. The 3–60-day averaged variance at the 0°, 180° site is 2.73×10^{-4} Pa^2 for zonal wind stress and 1.29×10^{-4} Pa^2 for meridional wind stress.

bands with longer periods, as was done in Harrison and Luther (1990). The broad peak in zonal wind energy in the 3–60-day bands, with a maximum in the 7–30-day bands, is nonetheless evident at all of these buoy locations. This confirms that enhanced zonal wind energy at these subseasonal periods is a characteristic of western-central equatorial Pacific open-ocean buoy, as well as low lying western-central Pacific island records.

Moving farther east along the equator, we see that the level of energy in zonal wind diminishes substantially (Fig. 2, top-center and top-right panels). Even in the central Pacific (170°, 155°, and 140°W) this is notable, with levels near 0.7 m^2 s^{-2} in the central Pacific versus levels >2 m^2 s^{-2} in the west. A meridional wind peak in the 3–7-day band with character and variance comparable to that seen in the western Pacific is still recognizable in the central Pacific, although it is more sharply peaked in the central than western basin.

In the eastern equatorial Pacific (125°, 110°, and 95°W; Fig. 2, right panels) the zonal wind energy in the 7–30-day band is essentially reduced to background variance levels of ~0.2 to 0.5 m^2 s^{-2}. The meridional wind energy peak is also basically gone. This region is relatively quiet, compared to the west, from the semiannual to 2-day period (the Nyquist frequency for daily average data).

Figure 3 summarizes the wind variance levels over the 3–60-day range for all the moored buoys, normalized against the variance at 0°, 180° ($U_{0°,180°} = 1.48$ m^2 s^{-2}; $V_{0°,180°} = 1.23$ m^2 s^{-2}). Zonal wind energy is maximum in the western tropical Pacific (variances at sites within 2°S–2°N, 147°–156°E average 2.66 m^2 s^{-2}). In the east, zonal wind energy at the moorings near the intertropical

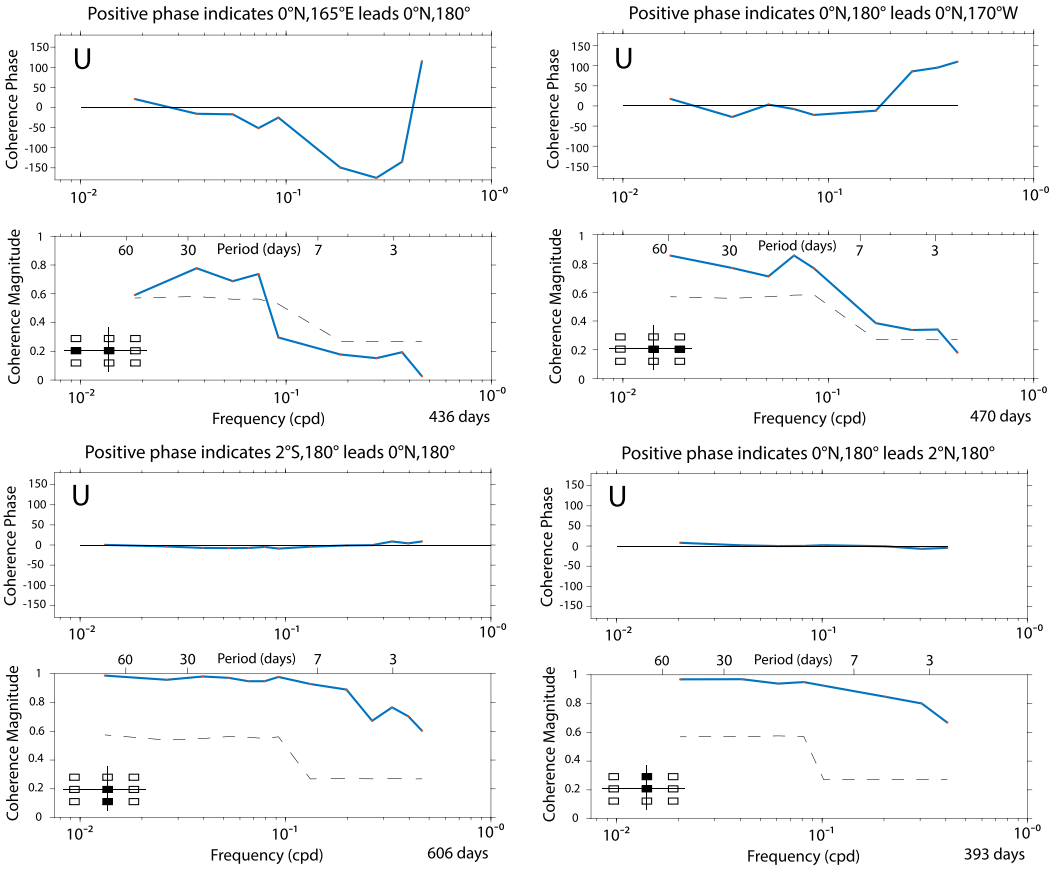

FIG. 5. Coherence phase and coherence magnitude of the zonal wind component around the 0°, 180° buoy. Results are based on (top left) 0°, 165°E and 0°, 180°; (top right) 0°, 180° and 0°, 170°W; (bottom left) 0°, 180° and 2°S, 180°; and (bottom right) 0°, 180° and 2°N, 180°. The dashed lines in the magnitude panels show the estimated 95% confidence statistical significance levels.

convergence zone (ITCZ) is larger than at the equator (mean at near-ITCZ sites along 8°N and east of 155°W is 1.68 $m^2 s^{-2}$, mean at equatorial 2°S–2°N sites east of 155°W is 0.81 $m^2 s^{-2}$). Observed zonal wind energy is smallest in the southeastern Pacific (mean over 5° and 8°S, east of 155°W is 0.34 $m^2 s^{-2}$). Meridional wind energy increases poleward of the equator in the west and near the ITCZ farther eastward (average of the 5° and 8°/9°N sites is 1.54 $m^2 s^{-2}$). As for zonal wind, the quietest moorings in terms of meridional wind energy are in the eastern equatorial and southeastern Pacific (5° and 8°S moorings, east of 155°W average 0.55 $m^2 s^{-2}$).

b. *Wind stress spectral results*

Figure 4 presents the spatial variation of 3–60-day band-averaged variance, relative to that at 0°, 180° for zonal and meridional wind stress ($\tau_{x\_0°,180°} = 2.73 \times 10^{-4}$ Pa^2; $\tau_{y\_0°,180°} = 1.29 \times 10^{-4}$ Pa^2). Zonal wind stress variances between 2°S and 2°N and from 156°E to 140°W are roughly comparable to one another (all of these sites are within 20% of their mean, with 10 of 16 within 10%). The far western equatorial Pacific does not dominate in zonal stress along the oceanic waveguide as it does in zonal wind, in which case the 2°S–2°N, 156°E results are 65%–95% larger than the mean calculated among the 2°S–2°N, 156°E–140°W sites. Between 5° and 8°N/S, 156°E and 140°W, zonal stress variance is comparable to or greater than at 0°, 180°. Only at 125°E and farther east is zonal stress variance substantially lower.

The meridional wind stress variance distribution along the core oceanic waveguide peaks at 0°, 180° where it is about 40% of the zonal stress variance. Meridional stress variance diminishes to the west and east of 180° longitude. It is, however, typically much greater at 5° and 8°N than in the waveguide, especially west of the 180°. These are the largest meridional stress variance values seen across the array (the 9°N, 140°W and 8°N, 110°W values are 2.4 times larger than at 0°, 180°).

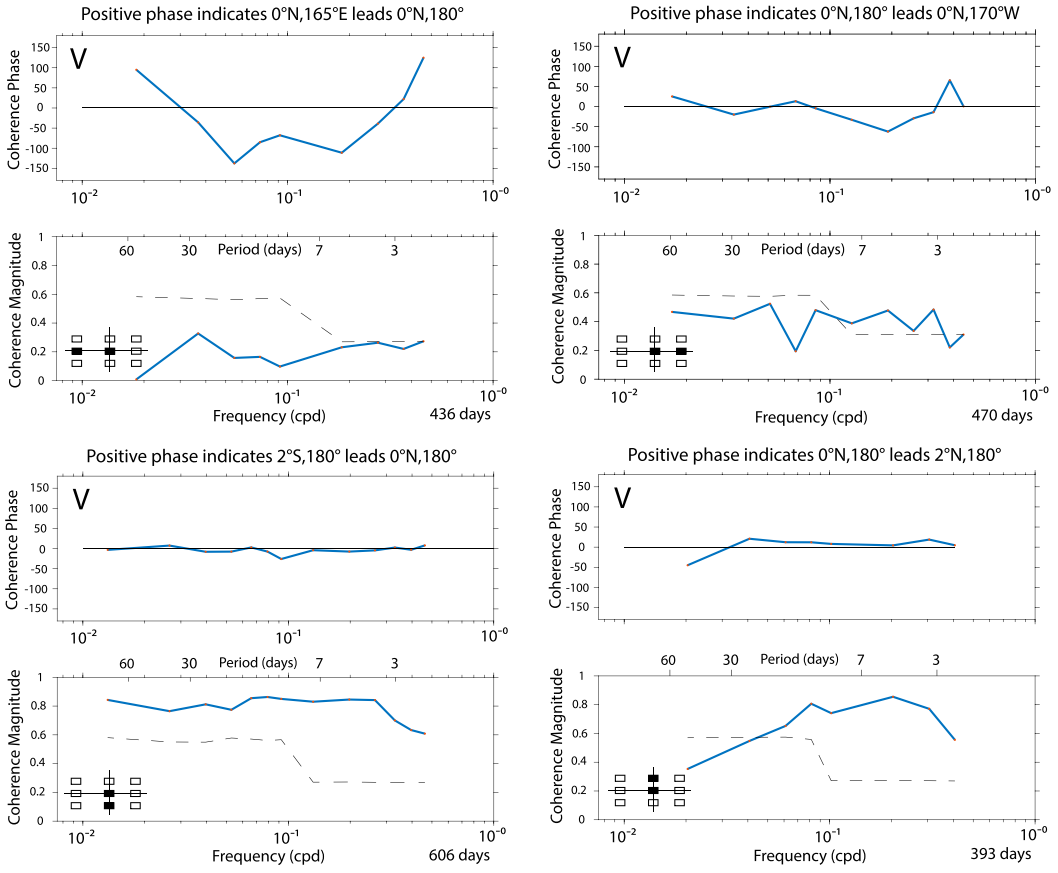

FIG. 6. As in Fig. 5, but for the meridional wind component.

c. *Wind and wind stress coherence results*

We begin with sample coherence results for five moorings centered at 0°, 180° from continuous records at least a year long (Figs. 5 and 6). For zonal wind, three of the four pairs considered show statistically significant (95% confidence) coherence values throughout the entire 3–60-day period frequency band, with near-zero phase at >5-day periods. The threshold significance level (dashed lines in Figs. 5 and 6) is 0.57 ± 0.01 for frequency < 0.1 cpd (averaging over eight adjacent bands) and 0.34 for frequency > 0.1 cpd (averaging over 25 adjacent bands). The remaining pair (0°, 165°E and 0°, 180°) is not highly coherent at sub-10-day periods but still has statistically significant coherence and near-zero phase from 10 days on. These results are substantially similar to those from islands in this region, as found by Harrison and Luther (1990). Meridional wind coherences are different in character than zonal winds; statistically significant values primarily are found in periods between about 2 days and 20 days, mostly with zero phase (Fig. 6). As in zonal wind, the pair involving 0°, 165°E has noticeably less coherence and more erratic phase results than the other three pairs involving 0°, 180°.

Figure 7 shows the spatial distribution of adjacent pair coherence, zonally and meridionally, for zonal wind and meridional wind averaged over the 3–60-day period frequency band. The meridional coherence is statistically significant (95% confidence) for almost every pair for zonal and meridional wind, and typically is greater than 0.7. Zonal coherence is smaller and not statistically significant at about half of the pairs for zonal wind and meridional wind but is statistically significant along the equator for zonal wind between 156°E and 125°W—albeit with amplitude of about 0.4, except for the 180°–170°W pair, which is 0.58.

The goal of the design of the buoy array was to be able to withstand loss of an adjacent mooring without great compromise in the resulting wind field. According to these results, loss of a zonal-neighbor mooring has more impact than loss of a meridional neighbor.

Coherence also was evaluated for pairs two buoys apart (Fig. 8). No zonally separated mooring pairs were found to have statistical significance in zonal wind or

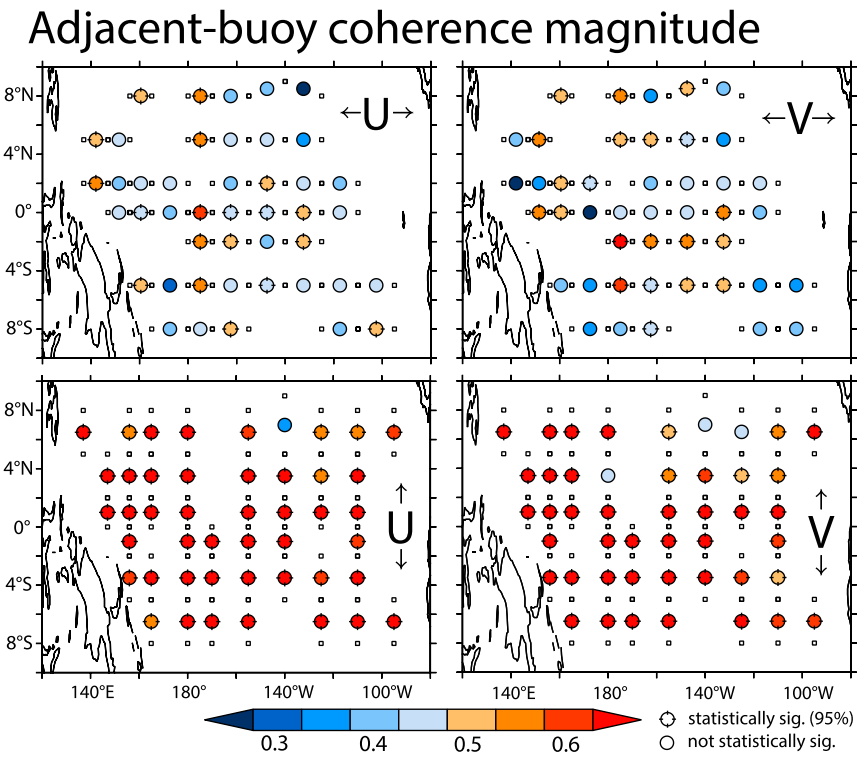

FIG. 7. Zonal and meridional wind coherence magnitudes between (left) zonal and (right) meridional pairs of moored buoys. Symbols lie at the centers of their buoy pairs. Statistical significance was calculated using Monte Carlo methods based on subsampling with replacement.

meridional wind. However, meridionally separated buoys were statistically coherent (95% confidence) for waveguide moorings. Evidently, the array design along most of the oceanic waveguide was more than minimally redundant meridionally for lost-buoy gap-filling. Even so, the array is unable to provide reliable curl information; resolving the detailed spatial and temporal structure of wind stress curl with buoys would require many more than are deployed at present.

Zonally and meridionally adjacent and two-buoy-apart coherence calculations were also made for zonal and meridional wind stress. Meridional coherence is statistically significant for almost every zonal and meridional wind stress pair (Fig. 9), and in this way similar to the wind coherence results (Fig. 7). The exceptions (those not statistically significant) are mostly found near the ITCZ.

For zonal wind stress, a second and third set of zonal and meridional coherences were calculated from the second and third longest continuous paired records available (see Fig. S1 in the online supplemental material). These additional results also show that zonal coherence is generally smaller than meridional coherence, with statistically significant (95%) zonal coherence of equatorial zonal wind stress found mainly between 165°E and 140°W. Evidently, the zonal spacing is insufficient to resolve the fetch of equatorial westerly wind events in their preferred western Pacific genesis region (Harrison and Vecchi 1997).

No pairs two buoys apart zonally were found to have coherence magnitude above 0.4 or be statistically significant (Fig. 10). Meridionally two-buoy-apart pairs were coherent within 5°S and 5°N for all such pairs in zonal wind stress and 20 of 22 pairs in meridional stress. The meridional spacing over the majority of the waveguide is better than minimally redundant (for mitigation of a single lost buoy) in wind and wind stress.

d. Special features of the 165°E–180° area

We noted above the lack of zonal coherence between the equatorial moorings at 165°E and 180°. This is noteworthy given the strong coherence found for the three other mooring pairings with the point 0°, 180°. A simple examination of the zonal wind time series from 0°, 165°E and 0°, 180° illustrates why (Fig. 11). There are several substantial westerly wind events at 165°E that either have no westerly

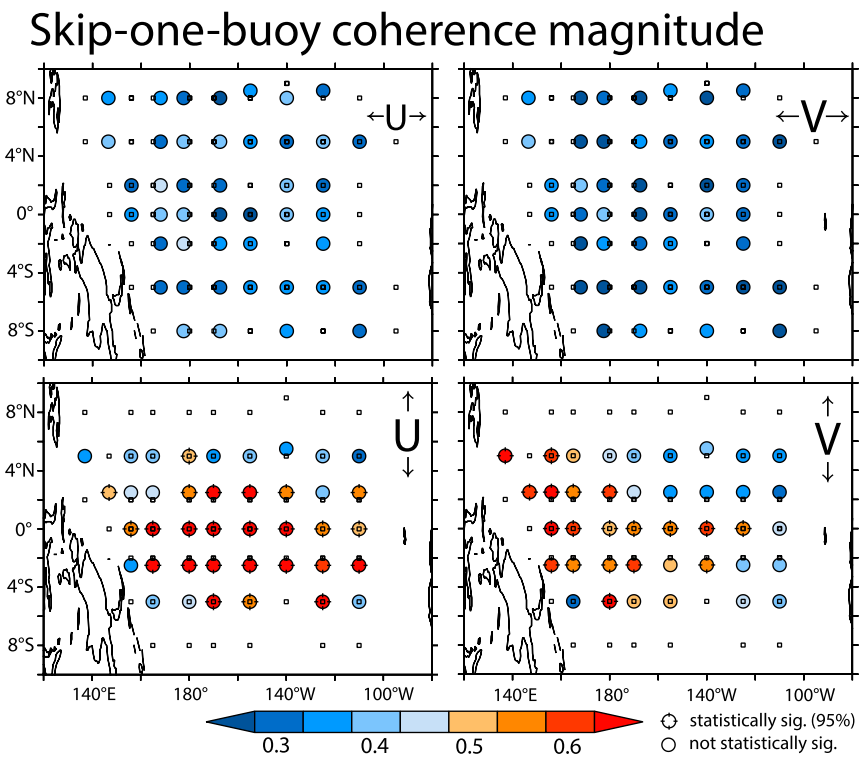

FIG. 8. As in Fig. 7, but for pairs two buoys apart.

counterpart at 180° or are paired with counteracting easterly winds farther east. Clearly the western equatorial Pacific needs to be carefully observed because the strong westerly wind events there can have profound impact on equatorial SST and subsurface warming farther east, provided that they are not countered by easterlies located farther east along the waveguide (Harrison and Chiodi 2009).

4. Discussion

The design of the TAO/TRITON moored array had to assume that the spectral density of variance and wind coherence characteristics calculated based on near–date line island data held across the tropical Pacific basin. Revisiting this assumption by calculating similar statistics based on the resulting moored-buoy array data has revealed, not unexpectedly, that these wind statistics change in character across the span of the array. In particular, the variance peak in the 7–30-day band in zonal wind found in low-lying western Pacific island records by Harrison and Luther (1990) is clearly seen in the western Pacific buoy wind records, but diminishes moving eastward in the oceanic equatorial waveguide. Adjacent-buoy zonal wind (wind stress) coherence is strongest just east of the date line on the equator, out to about 140°W (155°W), and diminishes toward the coasts. The goal of a minimum redundancy of mooring sites coherently sampling the wind variability field is not met across the waveguide by the original buoy spacing; increased zonal sampling is needed east of 140°W and west of the date line. Zonal winds west of the date line along the equator are often uncorrelated with date line zonal winds (this will be revisited below).

There is generally strong and statistically significant meridional coherence of zonal wind across the array, even for twice the present moored-buoy spacing. In terms of array resilience to the unexpected loss of a single mooring, sampling in the meridional direction across the waveguide is more than adequate.

There is much less meridional wind variance than zonal wind variance along the oceanic waveguide in the 7–30-day band. Meridional wind variance was found herein to be concentrated at frequencies around the 4-day period, which is consistent with the island results of Harrison and Luther (1990). Generally, meridional wind variance is maximum toward the ITCZ and South Pacific convergence zone (SPCZ). Coherence patterns of meridional wind are rather similar to those of zonal wind, although zonal coherence of meridional wind along the equator is weaker than zonal coherence of zonal wind from 165°E to 140°W. Meridional wind affects equatorial zonal stress characteristics through its role in determining wind speed.

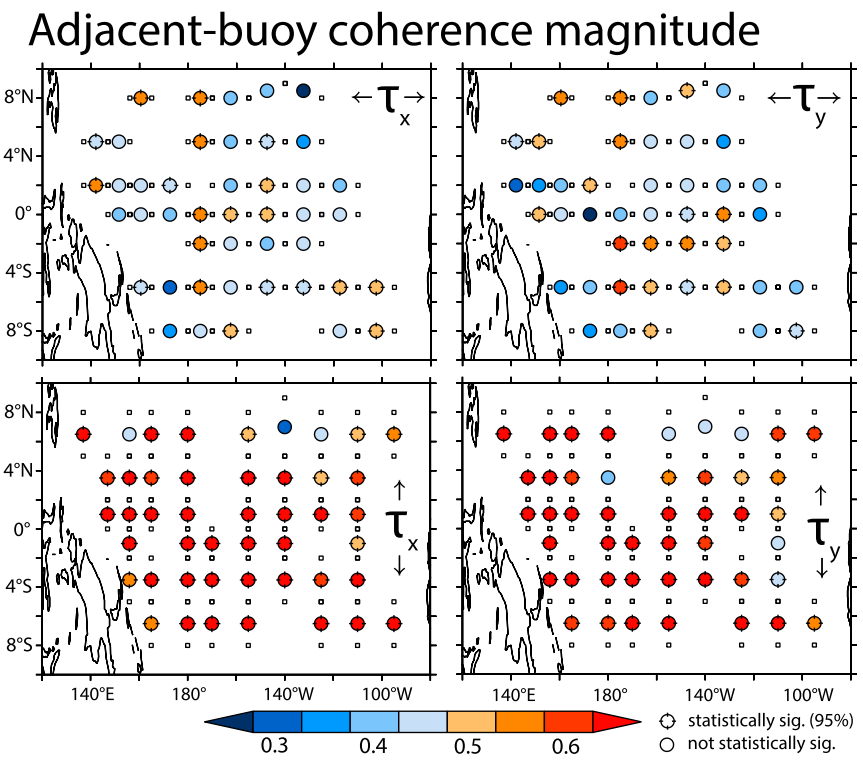

FIG. 9. As in Fig. 7, but for wind stress.

Zonal stress along the waveguide is less sharply peaked in frequency spectra than is zonal wind, largely because of the higher-frequency contributions from meridional wind. Substantial energy nonetheless remains in the 3–60-day band of zonal stress. The coherence patterns for stress are broadly similar to those for wind, but with somewhat lower coherence along the waveguide, except between the date line and 140°W. Adjacent-buoy wind stress coherence remains generally high in the meridional direction.

Efforts to hindcast and understand waveguide SST variability associated with both ENSO and the seasonal cycle depend critically on accurate wind stress information (Harrison et al. 1990, 2009; Kumar and Hu 2012). Recent studies have demonstrated that the TAO/TRITON array, when nearly fully reporting wind observations, provides usefully accurate (signal-to-noise > 2) hindcasts of Niño-3.4 SST anomalies (Chiodi and Harrison 2017b; Chiodi 2019). They have also demonstrated that gaps created by recent degradation of observations, such as occurred in 2012–14 when daily wind returns from TAO/TRITON fell by ~50% compared to the previous decade, have led to hindcast Niño-3.4 error comparable to the magnitude of the ENSO signal itself (Chiodi and Harrison 2017b).

Most recent ENSO studies have relied on analyzed wind products rather than the available direct observations for wind and wind stress information. The most commonly used analyses, such as the NCEP–NCAR reanalysis (Kalnay et al. 1996) or ERA-Interim (Dee et al. 2011), have been shown to contain substantially spurious representations of equatorial Pacific winds, relative to the direct observations, even with the observations available for assimilation into them. The spurious trend component in ERA-Interim was shown to induce a Niño-3.4 hindcast bias of ~2°C between start and end of the 1992–2011 period (Chiodi and Harrison 2017a). A similarly misleading trend component has been identified over the last 25 years in the satellite-focused Cross-Calibrated Multi-Platform wind product (CCMP; McGregor et al. 2017; Chiodi et al. 2019). Accurately estimating the variability and trend of tropical Pacific wind field characteristics over the last 25 years has required being able to resolve them with the TAO/TRITON mooring array.

There is hope that satellite wind observations, together with a diminished mooring array dataset, can produce satisfactory wind and wind stress fields for ENSO study and forecasting (TPOS 2020). Hindcast studies using historical satellite wind products demonstrate the need for significantly better satellite wind estimates than have been available since the QuikSCAT mission [Chiodi 2019; see Ricciardulli and Wentz (2015) for information

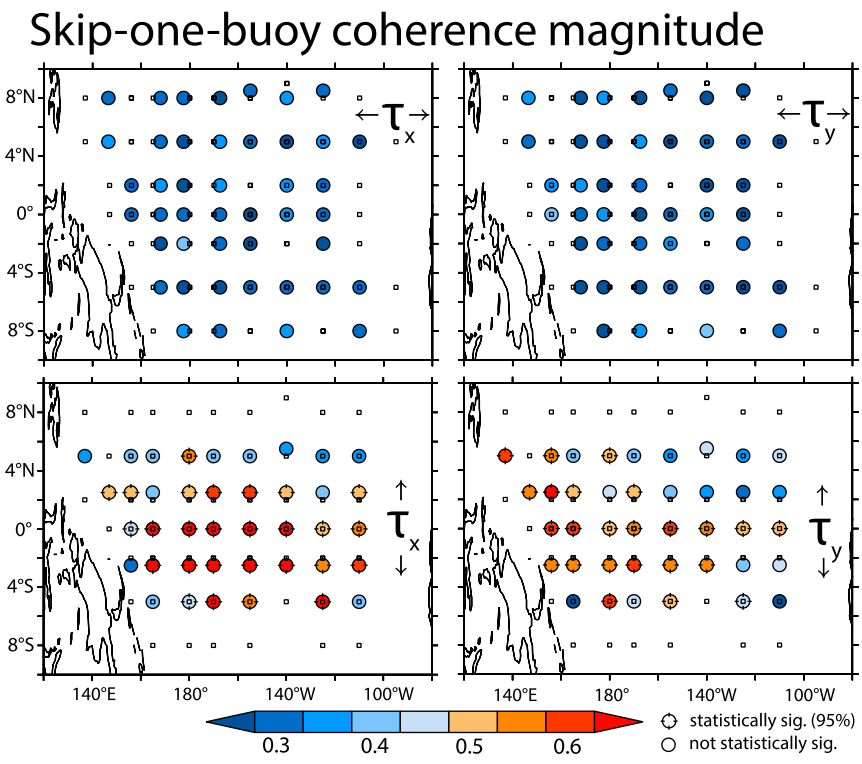

FIG. 10. As in Fig. 8, but for wind stress.

about QuikSCAT backscatter measurements and their processing to wind stress information]. To assume that future satellite missions will provide the needed wind estimates is, at present, to put at risk the effectiveness of the Tropical Pacific Observing System.

As the Tropical Pacific Ocean–Atmosphere Observing System is now being revised for the coming decade (TPOS 2020), it is timely to review the design of the mooring array. The results of this study reaffirm the design of the array over the oceanic waveguide between the date line and 140°W. They also highlight the importance of the zonal wind observations west of the date line, where zonal winds have been shown to not correlate well with date line winds. Examination of 165°E and 180° illustrated that westerly wind events observed at 165°E did not extend to the date line. This is consistent with the westerly wind event separation found by Harrison and Giese (1991) and Vecchi and Harrison (2000), which identified 180° as the boundary between the so-called central- and eastern-type westerly wind events.

Zonal winds at 180° can also be seen to occasionally oppose synoptic-scale westerly wind events observed at 165°. Harrison and Chiodi (2009) have shown that the amplitude and character of the SSTA warming driven by western Pacific westerly wind events is highly sensitive to the fetch and amplitude of this opposition. Particularly, being able to predict whether the WWE-driven warming will extend along the waveguide to the South American coast, as in the traditional El Niño composite (Rasmusson and Carpenter 1982; Larkin and Harrison 2002), or be trapped near the date line as in a central type of El Niño event (Larkin and Harrison 2005; Capotondi et al. 2015) depends upon having accurate observational knowledge of the wind variability field over this region. Reducing the zonal spacing of buoys east of the date line would improve our ability to do this.

The recent second report of TPOS 2020 proposes removing the 5° and 8°N/S TAO moorings along 125°W, 155°W, and 180° in favor of a more heavily instrumented array that extends farther north and south along other array longitudes (see Kessler et al. 2019, their Fig. 7.4). Were winds from adjacent buoy pairs uniformly coherent across the array, its original minimal redundancy of moorings would evenly compensate for the proposed removals. Inspection of the observed coherences results reveals that this is not so. For example, zonal stress variability at 5°S, 125°W is significantly coherent (at 95%) with four ''high priority'' moorings; two to its north, at 2°S, 125°W and 0°S, 125°W, and its two zonal neighbors at 5°S, 140°W and 5°S, 110°W. Observations from these would mitigate the effects of removing 5°S, 125°W. For some sites slated for removal, no such

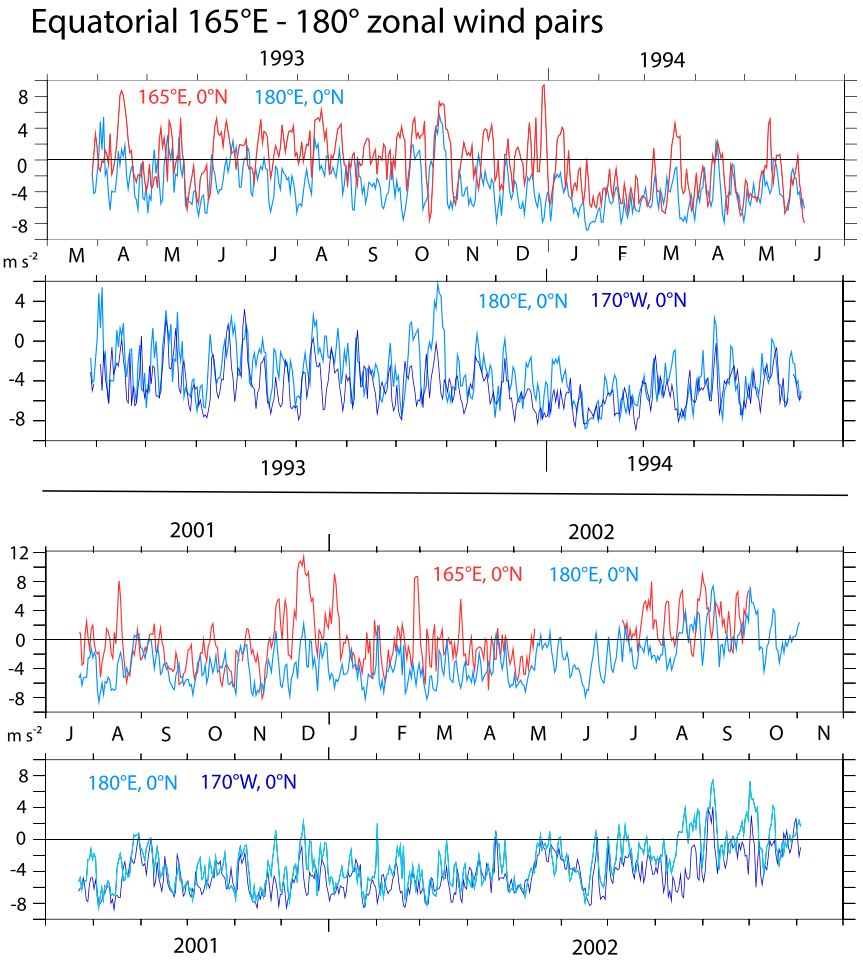

FIG. 11. Equatorial zonal wind pairs from 165°E and 180° and from 180° and 170°W. The 1993–94 (2001–02) segment is that from which the 0°, 165°E (0°, 180°) result in Fig. 7 was calculated.

compensation is evident (e.g., 8°S, 180°). For 5°N, 125°W we find only one such buoy, at 2°N, 125°W (the 5°N, 110°W pairing fails to yield >365 continuous days). And although statistically significant, the 2°–5°N, 125°W pair yields the smallest coherence observed among the eight 2°–5°N pairs shown in Fig. 9. Evidently the array has much less ability to compensate for the removal of 5°N, 125°W than 5°S, 125°W.

Further, with low coherence among its zonal neighbors, the 2°N, 125°W mooring will become unexpectedly critical for providing direct wind observations over the northern edge of the oceanic waveguide under the TPOS 2020 redesign (i.e., with 5°N, 125°W and 8°N, 125°W removed. Winds have been reported from 2°N, 125°W for ~80% of the days since TAO/TRITON was nominally completed in 1994. Successful efforts to increase the longevity of the anemometers deployed on such high priority moorings may be necessary to avoid 20% gaps in array coverage along the edges of the oceanic waveguide.

5. Conclusions

The original tropical Pacific moored-buoy array design assumption that the statistics calculated from western tropical Pacific island wind records are representative of open-ocean conditions and other regions of the tropical Pacific had not previously been thoroughly reexamined. We revisit the original moored-buoy array design calculations using the wind observations provided by the array since its basinwide deployment in the mid-1990s and find that the character of key wind statistics changes across the tropical Pacific basin in ways that could not be determined from the original island wind study.

In particular, the island results provided a best-case answer for mooring zonal spacing with minimally redundant coherence between adjacent buoys. Buoy zonal coherence scales are often shorter than determined from the islands. Buoy meridional coherence scales are longer than from the islands. This implies that reduced meridional sampling could still yield minimal redundancy but enhanced zonal sampling is needed to reach minimal redundancy. For zonal stress in particular, enhanced zonal sampling along the equator and west of the date line, as well as in the far eastern basin, is needed to reach minimal redundancy. Process study may be needed to determine optimal buoy spacing in these regions.

Acknowledgments. This study was supported by funding from the Ocean Observing and Monitoring Division of the NOAA Climate Program Office (FundRef 100007298), NOAA's Pacific Marine Environmental Laboratory (Contribution 5034), and the Joint Institute for the Study of the Atmosphere and Ocean under NOAA Cooperative Agreement NA15OAR4320063, Contribution 2019-1033. Helpful comments were provided by M. McPhaden and S. Hu, as well as two anonymous reviewers.

REFERENCES

Ando, K., and Coauthors, 2017: Fifteen years progress of the TRITON array in the western Pacific and eastern Indian Oceans. *J. Oceanogr.*, **73**, 403–426, https://doi.org/10.1007/s10872-017-0414-4.

Bendat, J. S., and A. G. Piersol, 1971: *Random Data: Analysis and Measurement Procedures*. Wiley-Interscience, 407 pp.

Bracewell, R. N., 1978: *The Fourier Transform and Its Applications*. 2nd ed. McGraw-Hill, 444 pp.

Capotondi, A., and Coauthors, 2015: Understanding ENSO diversity. *Bull. Amer. Meteor. Soc.*, **96**, 921–938, https://doi.org/10.1175/BAMS-D-13-00117.1.

Chiodi, A. M., 2019: Diagnosing and predicting ENSO SSTA development from moored-buoy and scatterometer winds. *J. Climate*, **32**, 8755–8770, https://doi.org/10.1175/JCLI-D-19-0183.1.

——, and D. E. Harrison, 2015: Equatorial Pacific easterly wind surges and the onset of La Niña events. *J. Climate*, **28**, 776–792, https://doi.org/10.1175/JCLI-D-14-00227.1.

——, and ——, 2017a: Observed El Niño SSTA development and the effects of easterly and westerly wind events in 2014/15. *J. Climate*, **30**, 1505–1519, https://doi.org/10.1175/JCLI-D-16-0385.1.

——, and ——, 2017b: Simulating ENSO SSTA from TAO/Triton winds: The impacts of 20 years of buoy observations in the Pacific waveguide and comparison with reanalysis products. *J. Climate*, **30**, 1041–1059, https://doi.org/10.1175/JCLI-D-15-0865.1.

——, J. P. Dunne, and D. E. Harrison, 2019: Estimating air–sea carbon flux over the tropical Pacific: Importance of winds and wind analysis uncertainty. *Global Biogeochem. Cycles*, **33**, 370–390, https://doi.org/10.1029/2018GB006047.

Dee, D. P., and Coauthors, 2011: The ERA-Interim reanalysis: configuration and performance of the data assimilation system. *Quart. J. Roy. Meteor. Soc.*, **137**, 553–597, https://doi.org/10.1002/qj.828.

Delcroix, T., G. Eldin, M. McPhaden, and A. Morliere, 1993: Effects of westerly wind bursts upon the western equatorial Pacific Ocean, February–April 1991. *J. Geophys. Res.*, **98**, 16 379–16 385, https://doi.org/10.1029/93JC01261.

Dunn, R. J. H., K. M. Willet, D. E. Parker, and L. Mitchell, 2016: Expanding HadISD: Quality-controlled, sub-daily station data from 1931. *Geosci. Instrum. Methods Data Syst.*, **5**, 473–491, https://doi.org/10.5194/gi-5-473-2016.

Eisenman, I., L. Yu, and E. Tziperman, 2005: Westerly wind bursts: ENSO's tail rather than the dog? *J. Climate*, **18**, 5224–5238, https://doi.org/10.1175/JCLI3588.1.

Feng, M., P. Hacker, and R. Lukas, 1998: Upper ocean heat and salt balances in response to a westerly wind burst in the western equatorial Pacific during TOGA COARE. *J. Geophys. Res.*, **103**, 10 289–10 311, https://doi.org/10.1029/97JC03286.

HadISD, 2009: Hadley Integrated Surface Dataset, version 3.0.1.201908p. Met Office Hadley Centre, accessed 22 April 2019, https://www.metoffice.gov.uk/hadobs/hadisd/.

Harrison, D. E., and D. S. Luther, 1990: Surface winds from tropical Pacific islands—Climatological statistics. *J. Climate*, **3**, 251–271, https://doi.org/10.1175/1520-0442(1990)003<0251:SWFTPI>2.0.CO;2.

——, and B. S. Giese, 1991: Episodes of surface westerly winds as observed from islands in the western tropical Pacific. *J. Geophys. Res.*, **96**, 3221–3237, https://doi.org/10.1029/90JC01775.

——, and G. A. Vecchi, 1997: Westerly wind events in the tropical Pacific, 1986–95. *J. Climate*, **10**, 3131–3156, https://doi.org/10.1175/1520-0442(1997)010<3131:WWEITT>2.0.CO;2.

——, and A. M. Chiodi, 2009: Pre- and post-1997/1998 westerly wind events and equatorial Pacific cold tongue warming. *J. Climate*, **22**, 568–581, https://doi.org/10.1175/2008JCLI2270.1.

——, B. S. Giese, and E. S. Sarachik, 1990: Mechanisms of SST change in the equatorial waveguide during the 1982–83 ENSO. *J. Climate*, **3**, 173–188, https://doi.org/10.1175/1520-0442(1990)003<0173:MOSCIT>2.0.CO;2.

——, A. M. Chiodi, and G. A. Vecchi, 2009: Effects of surface forcing on the seasonal cycle of the eastern equatorial Pacific. *J. Mar. Res.*, **67**, 701–729, https://doi.org/10.1357/002224009792006179.

Hartten, L. M., 1996: Synoptic settings of westerly wind bursts. *J. Geophys. Res.*, **101**, 16 997–17 019, https://doi.org/10.1029/96JD00030.

Josey, S. A., L. Yu, S. Gulev, X. Jin, N. Tilinina, B. Barnier, and L. Brodeau, 2014: Unexpected impacts of the Tropical Pacific array on reanalysis surface meteorology and heat fluxes. *Geophys. Res. Lett.*, **41**, 6213–6220, https://doi.org/10.1002/2014GL061302.

Kalnay, E., and Coauthors, 1996: The NCEP/NCAR 40-Year Reanalysis Project. *Bull. Amer. Meteor. Soc.*, **77**, 437–471, https://doi.org/10.1175/1520-0477(1996)077<0437:TNYRP>2.0.CO;2.

Keen, R. A., 1982: The role of cross-equatorial cyclone pairs in the Southern Oscillation. *Mon. Wea. Rev.*, **110**, 1405–1416, https://doi.org/10.1175/1520-0493(1982)110<1405:TROCET>2.0.CO;2.

Kessler, W.S., and Coauthors, 2019: Second report of TPOS 2020. GOOS-234, 265 pp., http://tpos2020.org/second-report/.

Kumar, A., and Z.-Z. Hu, 2012: Uncertainty in the ocean–atmosphere feedbacks associated with ENSO in the re-analysis products. *Climate Dyn.*, **39**, 575–588, https://doi.org/10.1007/s00382-011-1104-3.

Larkin, N. K., and D. E. Harrison, 2002: ENSO warm (El Niño) and cold (La Niña) event life cycles: Ocean surface anomaly patterns, their symmetries, asymmetries, and implications. *J. Climate*, **15**, 1118–1140, https://doi.org/10.1175/1520-0442(2002)015<1118:EWENOA>2.0.CO;2.

——, and ——, 2005: Global seasonal temperature and precipitation anomalies during El Niño autumn and winter. *Geophys. Res. Lett.*, **32**, L16705, https://doi.org/10.1029/2005GL022860.

Lengaigne, M., E. Guilyardi, J. P. Boulanger, C. Menkes, P. Delecluse, P. Inness, J. Cole, and J. Slingo, 2004: Triggering of El Niño by westerly wind events in a coupled general circulation model. *Climate Dyn.*, **23**, 601–620, https://doi.org/10.1007/s00382-004-0457-2.

McGregor, S., A. Sen Gupta, D. Dommenget, T. Lee, M. J. McPhaden, and W. S. Kessler, 2017: Factors influencing the skill of synthesized satellite wind products in the tropical Pacific. *J. Geophys. Res. Oceans*, **122**, 1072–1089, https://doi.org/10.1002/2016JC012340.

McPhaden, M. J., and Coauthors, 1998: The Tropical Ocean–Global Atmosphere (TOGA) observing system: A decade of progress. *J. Geophys. Res.*, **103**, 14 169–14 240, https://doi.org/10.1029/97JC02906.

——, A. J. Busalacchi, and D. L. T. Anderson, 2010: A TOGA retrospective. *Oceanography*, **23**, 86–103, https://doi.org/10.5670/oceanog.2010.26.

Rasmusson, E. M., and T. H. Carpenter, 1982: Variations in tropical sea surface temperature and surface wind fields associated with the Southern Oscillation/El Niño. *Mon. Wea. Rev.*, **110**, 354–384, https://doi.org/10.1175/1520-0493(1982)110<0354:VITSST>2.0.CO;2.

Ricciardulli, L., and F. J. Wentz, 2015: A scatterometer geophysical model function for climate-quality winds: QuikSCAT Ku-2011. *J. Atmos. Oceanic Technol.*, **32**, 1829–1846, https://doi.org/10.1175/JTECH-D-15-0008.1.

Smith, S. R., D. M. Legler, and K. V. Verzone, 2001: Quantifying uncertainties in NCEP reanalyses using high-quality research vessel observations. *J. Climate*, **14**, 4062–4072, https://doi.org/10.1175/1520-0442(2001)014<4062:QUINRU>2.0.CO;2.

TAO/TRITON, 2000: Tropical Atmosphere Ocean/Triangle Trans-Ocean Buoy Network. NOAA Pacific Marine Environmental Laboratory TAO project office, accessed 3 January 2018, https://www.pmel.noaa.gov/tao/drupal//disdel/.

Vecchi, G. A., and D. E. Harrison, 2000: Tropical Pacific sea surface temperature anomalies, El Niño, and equatorial westerly wind events. *J. Climate*, **13**, 1814–1830, https://doi.org/10.1175/1520-0442(2000)013<1814:TPSSTA>2.0.CO;2.

Wittenberg, A. T., 2004: Extended wind stress analyses for ENSO. *J. Climate*, **17**, 2526–2540, https://doi.org/10.1175/1520-0442(2004)017<2526:EWSAFE>2.0.CO;2.